



Published in final edited form as:

J Phys Chem B. 2015 February 19; 119(7): 2886–2896. doi:10.1021/jp511758w.

Probing the Sources of the Apparent Irreproducibility of Amyloid Formation: Drastic Changes in Kinetics and a Switch in Mechanism due to Micelle-Like Oligomer Formation at Critical Concentrations of IAPP

Jeffrey R. Brender^{1,†}, Janarthanan Krishnamoorthy^{1,†}, Michele F. M. Sciacca^{1,2,†}, Subramanian Vivekanandan¹, Luisa D'Urso², Jennifer Chen¹, Carmelo La Rosa², Ayyalusamy Ramamoorthy^{1,*}

¹Biophysics, University of Michigan, Ann Arbor, Michigan

²Department of Chemical Sciences, University of Catania, Catania, Italy

Abstract

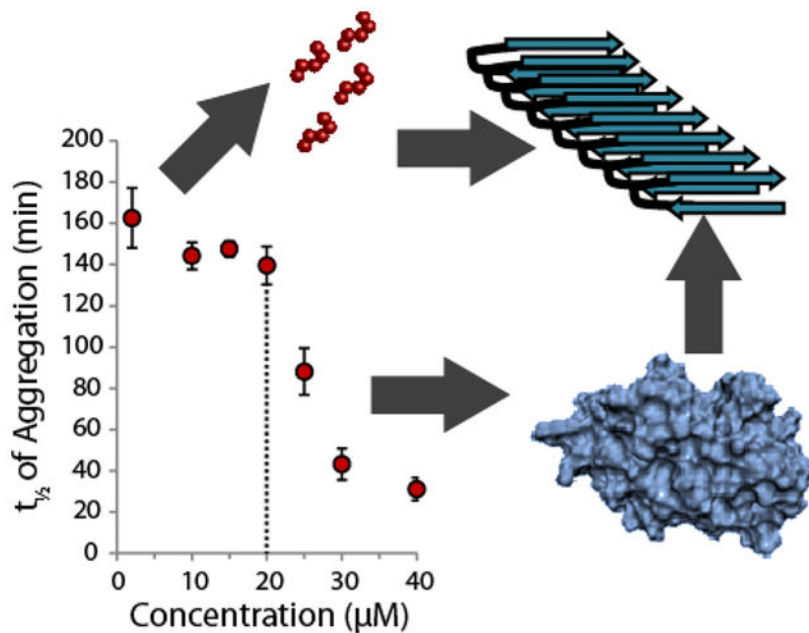
The aggregation of amyloidogenic proteins is infamous for being highly chaotic, with small variations in conditions sometimes leading to large changes in aggregation rates. Using the amyloidogenic protein IAPP (Islet Amyloid Polypeptide Protein, also known as amylin) as an example, we show that a part of this phenomenon may be related to the formation of micelle-like oligomers at specific critical concentrations and temperatures. We show pyrene fluorescence can sensitively detect micelle-like oligomer formation by IAPP and discriminate between micelle-like oligomers from fibers and monomers, making pyrene one of the few chemical probes specific for a prefibrillar oligomer. We further show oligomers of this type reversibly form at critical concentrations in the low micromolar range and at specific critical temperatures. Micelle-like oligomer formation has several consequences for amyloid formation by IAPP. First, the kinetics of fiber formation increase substantially as the critical concentration is approached but are nearly independent of concentration below it, suggesting a direct role for the oligomers in fiber formation. Second, the critical concentration is strongly correlated with the propensity to form amyloid: higher critical concentrations are observed for both IAPP variants with lower amyloidogenicity and for native IAPP at acidic pH in which aggregation is greatly slowed. Furthermore, using the DEST NMR technique, we show the pathway of amyloid formation switches as the critical point is approached, with self-interactions primarily near the N-terminus below the critical temperature and near the central region above the critical temperature, reconciling two apparently conflicting views of the initiation of IAPP aggregation.

Graphical Abstract

*Corresponding Author: Ayyalusamy Ramamoorthy, 930 N. University Avenue, Ann Arbor, Michigan 48109-1055 (USA), ramamoor@umich.edu.

†These authors contributed equally to this work

Supporting Information: Materials and methods, time courses for the thioflavin T experiment, log-log transform of the $t_{1/2}$ values from the thioflavin T experiment, ¹⁵N SOFAST-HMQC spectra of hIAPP free acid after a return to 4° after the temperature jump. This material is available free of charge via the Internet at <http://pubs.acs.org>.



Keywords

intermediates; islet amyloid polypeptide; prefibrillar; aggregation; protein misfolding; structural biophysics

Introduction

Inappropriate, uncontrolled protein aggregation is emerging as a common thread linking many types of common pathologies, including some very common and currently incurable disorders.¹ The most widespread type of aggregation is the irreversible conversion of monomeric proteins into long fibers with a characteristic β -sheet structure known as amyloids.²⁻³ Because of the purported involvement of amyloidogenic proteins of this type in Alzheimer's and other very serious neurodegenerative disorders, considerable effort has been made to understand the process of amyloid formation with the intent of developing approaches to stop it.⁴⁻⁵

Unfortunately, progress in this area has been partially stymied by the seeming irreproducibility of many results.⁶⁻⁸ There have been several recent high profile examples where an apparent success has been replicated with mixed outcomes.⁹⁻¹⁴ The use of controlled *in vitro* conditions allows certain questions to be answered in a more precise manner.⁸ However, even under controlled *in vitro* conditions, a consensus is lacking for many amyloidogenic proteins on the specific mechanisms involved in amyloid formation.¹⁵⁻¹⁷ The lack of consensus on mechanism and the complex nature of the various species along the aggregation pathway has proven frustrating for drug development, as many such drugs seek to target specific oligomers along the aggregation pathway.^{5, 18-19} Part of the lack of consensus appears to stem from the sensitivity of both the kinetics and mechanism to apparently minor changes in environmental conditions. Even minor changes, such as a buffer

substitution,^{20–21} can lead to substantial changes in pathway and intermediates. However, while early reports suggested amyloid formation may be truly random, controlled by the stochastic generation of an extremely limited number of seeding nuclei,⁶ later research has shown that the apparent irreproducibility of many amyloids can be tamed by a careful consideration of starting conditions and knowledge of the factors influencing aggregation.^{7, 22–25} Using the amyloidogenic peptide IAPP as a model system, we show that relatively small changes in concentration and temperature can cause large but reproducible changes in both the rate and mechanism of aggregation through the reversible formation of specific types of oligomers.

Materials and Methods

See the Supporting Information for detailed experimental procedures.

Results

The Rate of Fiber Formation by IAPP is Nearly Independent of Concentration below a Threshold Concentration

To gain insight into some of the factors that may cause such sensitivity to environmental conditions, we first looked at the concentration dependence of amyloid formation in the model amyloid protein IAPP by using the amyloid specific dye thioflavin T (ThT). Islet amyloid polypeptide (IAPP, sequence KCNTATCATQRLANFLVHSSNFGAILSSTNVGSNTY-NH₂ with an amidated C-terminus and a disulfide bridge between residues 2–7) is a peptide hormone whose pathological aggregation has been implicated in the development of type II diabetes.²⁶ IAPP is also frequently used as a model for amyloid formation from natively unstructured proteins, an important class of amyloidogenic proteins that also includes A β (implicated in Alzheimer's disease) and α -synuclein (Parkinson's).²⁷

The results of the ThT assay are shown in Fig. 1 with the time to half completion of fiber formation ($t_{1/2}$) plotted on the y-axis. The full time courses for the ThT assay can be found as Fig. S1 in the Supporting Information. For these experiments, two different forms of IAPP were used, the native human peptide which is amidated at the C-terminus (hIAPP) and the free acid form of the peptide (hIAPP free acid), which is known to aggregate slower than the native peptide.²⁸ The reason for this difference between the free acid and amidated forms is currently unclear, but may be related either to an increase in electrostatic repulsion in the free acid form,²⁹ the folding of the C-terminus against His18 in the free acid form,^{29–30} or to a difference in the rigidity of the C-terminus between the free acid and amidated forms of hIAPP.^{31–32} All three measures of fiber formation kinetics reveal an unusual feature for both peptides: fiber formation is nearly independent of peptide concentration below a specific concentration, which we define as a “threshold concentration” for aggregation (~ 1 μ M for hIAPP and 15 μ M for hIAPP free acid in this experiment, dashed lines in Fig. 1).

The Rate of Fiber Formation by IAPP Increases Sharply at a Threshold Concentration

Another look at the ThT kinetics reveals an even more striking feature. While fiber formation is nearly independent of concentration at low concentrations, the rate of fiber

formation sharply increases at the threshold concentration. The sharp changes apparent at the threshold concentration are unexpected, as most (but not all)^{33–36} current theories of amyloid formation predict a power law dependence of the fibrillization rate on the initial concentration.³⁵ In particular, the nucleation dependent polymerization theory commonly used to model amyloid formation predicts the rate-determining step is the buildup of an energetically unfavorable nucleus of size n during the lag phase.³⁷ After this buildup, aggregation proceeds quickly, leading to the characteristic sigmoidal shape of the kinetics of most amyloidogenic proteins. If IAPP aggregation follows such a mechanism, the concentration dependence of $t_{1/2}$ should follow the power law distribution αc^β where the exponent β is dependent on the nucleus size.^{35, 38} This power law relationship should translate to a smooth decrease of the aggregation time $t_{1/2}$ with increasing concentrations of hIAPP. While this power law relationship is roughly apparent above the threshold concentration (see Fig. S2), near the threshold concentration the kinetics sharply deviates from the expected values. This deviation suggests some other mechanism affects aggregation that is not accounted for in the traditional nucleation dependent polymerization model and is explored in more detail below.

Micelle-like hIAPP Oligomers Form near a Critical Micellar Concentration that Can Be Detected Sensitively and Specifically by Pyrene Fluorescence

Specifically, the existence of a threshold concentration is reminiscent of micelle formation. Micelle-like oligomers have been suggested to be intermediates along the aggregation pathway of A β ,^{33–34, 39} another amyloidogenic peptide that shares many properties with hIAPP.^{33–34, 40} For IAPP specifically, a short fragment of hIAPP free acid (hIAPP_{20–29}) has been proven to form micelles⁴¹ and micelle formation by full-length hIAPP has been theoretically predicted based on kinetic modeling.^{42–43} In particular, the formation of off-pathway micelles or other aggregates has been proposed to explain the apparent concentration independence of hIAPP aggregation.^{41, 43–44} The low concentrations involved (most previous measurements have used in excess of 5 μ M hIAPP) made directly detecting concentration dependent self-association by dynamic light scattering difficult. Instead, we employed pyrene fluorescence experiments to probe the formation of hydrophobic clusters by peptide self-association at a series of concentrations. The fluorescence emission spectrum of pyrene is environmentally sensitive with the ratio of the fluorescence intensities of the first (I_I) and third (I_{III}) vibronic bands decreasing as the hydrophobicity of the environment increases (Fig. 2A).⁴⁵ In particular, a decrease in the first band intensity and an increase in the third band indicate the formation of a micelle-like structure. In analogy to previous experiments on detergent micelles, an apparent CMC where the disordered monomer aggregates to form a micelle with a hydrophobic interior can therefore be defined by the inflection point in a plot of this ratio as a function of protein concentration.^{40, 46}

Both hIAPP and hIAPP free acid solutions show a sharp reduction in the I_I/I_{III} ratio as a threshold concentration is approached. hIAPP at pH 7.4 shows this this apparent CMC is near 2 μ M (Fig 2B black circles, the full pyrene spectrum is shown in Fig. 2A), which is close to the apparent critical micellar concentration (CMC) of the hIAPP_{20–29} fragment obtained by other means⁴¹ (3.5 μ M) and close to theoretical predictions for the CMC of hIAPP itself based on kinetic modeling (\sim 1.3–1.5 μ M).^{42–43} A similar experiment performed

using the free acid form of hIAPP (Fig. 2C) gives a higher threshold concentration of ~ 15 μM . Notably, the pyrene emission experiment is only sensitive to the formation of micellar oligomeric species of hIAPP. No change in the $I_{\text{I}}/I_{\text{III}}$ bands intensity ratio was observed by titrating the pyrene solution with preformed fibers of hIAPP (Figure 2B red circles), which suggests that pyrene has the rare property among chemical probes of being almost completely selective for non-fibrillar oligomer forms over amyloid fibers.⁴⁷

Micelle-Like Oligomer Formation is Reversible with Changes in Concentration and Temperature

Micelles formed from detergents and other amphiphilic compounds are usually dynamic structures with rapid exchange occurring between the micelle and monomer subunits in solution. Because of this rapid exchange between the monomer and micelle, dilution beyond the CMC usually results in the immediate dissociation of the micelle. For some micelles, critical solution temperatures also exist which control the formation of the micelle; micelles do not form above the upper critical solution temperature or below the lower critical solution temperature.⁴⁸ The dynamic nature of micelles contrasts markedly from the high kinetic stability of amyloid fibers and many types of oligomeric proteins. For example, stable populations of certain types of oligomers can be isolated by size exclusion chromatography,⁴⁹ a feat that would be difficult⁵⁰⁻⁵¹ if equilibrium was rapidly re-established as it is for micellar-type aggregates.

We first tested the reversibility of the formation of hIAPP micellar oligomers by diluting a sample of hIAPP above the threshold concentration and comparing the pyrene $I_{\text{I}}/I_{\text{III}}$ ratio with that obtained by titrating in hIAPP. If the oligomer can rapidly dissociate like a micelle, the dilution and titration curves should be identical. On the other hand, if the oligomers are kinetically stable like amyloid protofibrils, the $I_{\text{I}}/I_{\text{III}}$ ratio will not decrease as the sample is diluted. When a 4 μM sample of hIAPP is progressively diluted the pyrene $I_{\text{I}}/I_{\text{III}}$ ratios obtained by titration and dilution closely match (Fig. 3), indicating the formation of micelle-like oligomers hIAPP is a reversible process.

We next sought to see if a critical temperature for micelle-like oligomer formation exists by fixing the concentration of hIAPP above the threshold concentration at 4 μM and measuring the pyrene $I_{\text{I}}/I_{\text{III}}$ ratio as a function of temperature (Fig. 4) at pH 7.3. The plot clearly indicates that the formation of micelle-like oligomers does not occur at temperature below 10 $^{\circ}\text{C}$, indicating sample concentration by itself is not sufficient to induce oligomer formation. The $I_{\text{I}}/I_{\text{III}}$ ratio of pyrene in the absence of hIAPP did not change with temperature, confirming the fluorescence change is the result of oligomer formation and not temperature-dependent changes in fluorescence. For further confirmation, we checked the temperature dependence of the peak intensity in the ^{15}N -SOFAST HMQC spectra of hIAPP free acid (Fig. 5), as it is expected that oligomer formation will lead to a decrease in intensity either due to creation of NMR invisible oligomers at the expense of NMR visible monomers or due to line broadening from conformational exchange. At pH 5, where no oligomers were detected by pyrene, intensity increases with temperature in the ^{15}N -SOFAST HMQC spectra, as is typically observed with many disordered peptides and proteins.⁵² By contrast, at pH 7.3 the intensity drops abruptly at 10 $^{\circ}\text{C}$, identical to the

pyrene results. Decreasing the temperature from 30 to 4 °C almost entirely reverses the intensity changes (Fig. S3), strongly indicating that oligomer formation is reversible with temperature as well as concentration.

The Apparent CMC for Oligomer Formation Correlates with Amyloidogenic Propensity

When the results of the ThT aggregation assay (Figs. 1) are compared to the pyrene fluorescence results, it can be seen that $t_{1/2}$ clearly clusters into two regimes with the dividing line near the CMC as determined by the pyrene fluorescence assay. Below the CMC, $t_{1/2}$ is nearly independent of concentration. At the CMC, $t_{1/2}$ declines sharply as the concentration is increased. This particular type of concentration dependence suggests two separate mechanisms of aggregation are operational above and below the apparent CMC value.

A comparison of Figures 1 and 2 also reveals a possible relationship between the threshold concentration and the amyloidogenic propensity. The free acid form of hIAPP has a higher CMC than hIAPP (~15 μ M vs. ~1.5 μ M). Interestingly, the ThT experiments also show aggregation of the free acid form of hIAPP is significantly slower below the CMC than hIAPP, but similar the rates of both peptides are similar above the CMC.

We further explored this correlation between the aggregation rate and threshold concentration for oligomer formation by using variants of IAPP with significantly slower aggregation rates and pH ranges in which aggregation is significantly slowed. The rat variant of IAPP (rIAPP, sequence KCNTATCATQRLANFLVRSSNNLGPVLPPTNVGSNTY-NH₂; residues different than hIAPP are in bold) is normally non-amyloidogenic and non-toxic to cells.⁵³⁻⁵⁴ As expected, rIAPP did not form oligomers over the concentration range tested (Fig. 6 green circles). Similarly, the N-terminal 1–19 fragment of hIAPP (hIAPP₁₋₁₉) is significantly less amyloidogenic than the full-length peptide. While the 1–19 region of hIAPP is believed to be involved in peptide self-association, hIAPP₁₋₁₉ itself forms amyloid slowly and only at high (mM) concentrations.⁵⁵ Like rIAPP, hIAPP₁₋₁₉ did not form oligomers over the concentration range tested (Fig. 6). Finally, we tested for possible oligomer formation of hIAPP at pH 5. At this pH, His18 is protonated and it has been observed by multiple groups that fiber formation is significantly slower at pH 5 than at pH 7.3. Like the less amyloidogenic hIAPP₁₋₁₉ and rIAPP variants at pH 7.3, micelle-like oligomers of hIAPP did not form at pH 5 over the concentration range tested (Fig. 6 green circles)

IAPP Forms Distinctly Different Oligomers Above and Below the Critical Temperature and Concentration

The existence of separate fast and slow regimes suggests aggregation may proceed by a different mechanism above and below the critical concentration and temperature. To gain atomic level insight into the process of oligomer formation, we first acquired ¹H NMR spectra of the free acid form of hIAPP above (40 μ M) and below (10 μ M) the apparent CMC from the pyrene experiments at 37 °C and pH 7.3 (Fig. 7). Differences in the normalized spectra are immediately apparent. First, the average intensity is higher at 10 μ M than 40 μ M once both spectra are normalized for concentration (Fig. 7B). Since the signal from slowly

tumbling large oligomers would be broadened beyond detection, the increase in intensity upon dilution is consistent with the formation of large oligomers that are immediately dissociate upon dilution, consistent with the pyrene fluorescence results. Furthermore, the increase in intensity upon dilution is not uniform. Instead, the largest overall changes are in the aliphatic region of the spectrum, consistent with the involvement of the side-chains of hydrophobic residues in micelle-like oligomer formation. In particular, several peaks in this region are noticeably narrower, more intense, or shifted in frequency in the low concentration spectra. This finding is consistent with a micelle-like oligomer formation, as hydrophobic side-chains facing the interior of the micelle are expected to be more strongly perturbed than the hydrophilic side-chains facing the outside. It is important to note that all NMR experiments were performed in Shigemi tubes which lack a bulk air-water interface, indicating a bulk-air water interface is apparently not essential for either concentration or temperature dependent oligomer formation.

It has been shown previously for a variety of amyloidogenic proteins^{56–59} including hIAPP⁶⁰ that strongly shielded, broad peaks in the region 0.2 to –1 ppm correspond to the mobile side-chains in an oligomeric complex (Fig. 7 inset). Interestingly, at pH 7.3, but below the CMC, an additional peak can be seen in this region at 0.16 ppm that disappears as the concentration is increased. This finding suggests that another type of oligomer may be present at pH 7.3 at low concentration that is unobservable as the concentration is raised.

While the NMR results suggest an additional oligomer not detected by pyrene may form at low concentrations of IAPP at pH 7.3 but not pH 5, the results are not conclusive as this peak may only reflect collapsed states of the IAPP monomer,⁶⁰ differences in hydrogen exchange rates, and other factors. To more directly probe the existence of other types of oligomers, we directly visualized the aggregates formed during incubation above (25 °C) and below (4 °C) the critical temperature using AFM (Fig. 8). In this experiment, IAPP is first dissolved at pH 5 at either 25 °C or below 4 °C before the pH is quickly adjusted to pH 7.3 and the sample immediately deposited on mica. At 25 °C, a large population approximately spherical oligomers of approximately 12–15 nm radius along with another population of elongated oligomers are apparent immediately after incubation (see Fig. 8B and D). Oligomers of this type were not present when the sample was incubated at 4 °C. Instead, a close inspection of the high resolution AFM images of hIAPP incubated at 4 °C show a smaller population of a different type of oligomer, disc-like in shape with a height of approximately 1 nm but with a similar diameter as the 25 °C oligomers (Fig. 8A and C). We therefore conclude at least two distinct populations of oligomers likely exist above the critical temperature and threshold concentration, one of which is not detectable below either limit.

IAPP Self-Association is Primarily at the N-Terminus Below the Critical Temperature and in the Central Amyloidogenic Region Above the Critical Temperature

The existence of distinct types of oligomers above and below the critical concentration and temperature suggests different interactions and possibly different mechanisms maybe involved in fiber formation. We tested this possibility by probing the interactions of the monomer with the oligomer by Dark Exchange Saturation Transfer (DEST) NMR

experiments.^{61–63} In the DEST experiment (and related off-resonance⁶⁴ and saturation transfer experiments^{65–69}), the line broadening in the monomer spectrum caused by the association of the monomer with the oligomer is used as a probe to detect self-association sites within the hIAPP peptide. A weak RF field is applied far off-resonance to saturate the underlying but invisible oligomer states. The bound monomer has a significantly higher transverse relaxation rate (R_2) than the free monomer because of the longer rotational correlation time among other factors, which is reflected in a broader linewidth and decrease in intensity when it dissociates from the oligomer. This increase in R_2 is residue specific, residues which are not in contact with the oligomer and do not have their motion restricted by binding have smaller changes in R_2 . Considering that a large number of possible bound conformations exist, the magnitude of the changes in R_2 therefore report on the fraction of conformations in which that residue is bound.⁶² As a consequence, larger decreases in intensity upon saturation in the DEST experiment reflect regions of the hIAPP monomer having stronger contacts with the hIAPP oligomer.

In the original DEST experiment performed on a A β monomer protofibril system, the RF offset was varied to solve the full McConnell relaxation equations to get not only changes in R_2 but also the kinetic constants relating the equilibria.⁶² Unfortunately, hIAPP is considerably less stable than A β and it was impossible to collect enough points to solve the McConnell relaxation equations before the effects of aggregation became apparent. Instead, the data was interpreted semi-quantitatively using the decrease in intensity at given offsets due to saturation of the underlying invisible oligomer state.

Notwithstanding, clear trends emerged with the DEST-like experiment as a function of temperature and pH. At pH 5 and 4 °C where aggregation is slowest and both the pyrene (Fig. 6) and NMR experiments (Fig. 5 B and C) fail to detect oligomers, no decrease in intensity was detected for any residue in the DEST profile (Fig. 9A left and 9B top). The DEST experiment at low pH below the critical temperature therefore serves as a negative control to confirm intensity changes upon saturation are not present in the absence of oligomers in the DEST experiment.

The DEST profile changes when the experiment is performed at pH 7.3 but below the critical temperature (4 °C). Under this condition, micelle-like oligomers were not detected by the pyrene (Fig. 4) or the NMR experiments (Fig. 5). However, the AFM experiments suggest a separate type of oligomer, substantially smaller than the micelle-like oligomer, may exist (Fig. 8A). The intensities of resonances corresponding to residues at the N-terminal region of the peptide (residues 9–15) decrease moderately upon off resonance saturation, while the C-terminus and middle regions of the peptide (residues 16–37) show almost no change (Fig. 9A middle and 9B middle). Overall, the data support primarily N-terminal association at low temperatures with minimal involvement of the C-terminus.

A substantially different pattern was obtained near the critical temperature (10 °C). First, the overall intensity of all resonances is greatly reduced upon off-resonance excitation with effects seen further off-resonance than at 4 °C. The decrease in overall intensity indicates stronger self-association occurs at 10 °C than at 4 °C, in agreement with the pyrene, NMR, and AFM experiments. Unfortunately, the decrease in intensity with the increase in

temperature makes certain resonances undetectable and complications begin to arise from aggregation during the experiment. Nevertheless, although the pattern is not as clear as it is at 4 °C, the self-association appears to be centered at a different set of residues at 10 °C than 4 °C with residues 12–21 decreasing more than other residues after off-resonance saturation (Fig. 9B bottom). In the C-terminus, most of the residues are only moderately affected, with the notable exceptions of N31 and A25-L27, which is a region known to be important for fibrillogenesis⁷⁰ and is involved in the early formation of transient β -sheet oligomers.⁷¹ This pattern suggests a shift from the N-terminal contacts observed at 4 °C (primarily residues 9–15) towards interactions closer to the center of the peptide (primarily residues 12–21) as the sample is heated to near the critical temperature needed for micelle-like oligomer formation.

Discussion

We have shown here that the hIAPP amyloid protein, a model for other unstructured amyloid proteins in many (but not all) respects: 1) reversibly forms micelle like aggregates in a manner sharply dependent on hIAPP concentration and temperature 2) rapidly forms fibers above the concentration needed for the formation of micelle-like oligomers and more slowly below it 3) shows a different self-association pattern at the atomic level in the early stages of aggregation when micelle-like oligomers are present. Micelle formation has previously been proposed as an off-pathway intermediate for hIAPP based on the apparent concentration independence of aggregation.^{41, 43–44} While a detailed quantitative understanding still awaits further experimental verification in light of the many kinetic variables involved, our results suggest a more complicated picture with at least two separate mechanisms for nucleation: a less efficient process occurring within small oligomers dominated by N-terminal self-association and a more efficient process initiated within micelle-like oligomers involving more extensive contacts throughout the peptide.

Differences between IAPP micelles and detergent-like micelles

Although the “micelle-like” hIAPP oligomers described above share many properties in common with traditional micelles, it is important to recognize several differences between them and simple spherical micelles such as those formed by detergents. For example, in a detergent micelle system the concentration of monomers above the CMC is typically close to the CMC value.⁴⁸ Theoretically, this relationship arises from the strong cooperativity assembly of detergent micelles and the packing restrictions present within the micelle, which limits the micelle size to specific limits ($< \sim 100$ molecules).⁴⁸ Although the actual concentration of hIAPP monomers is difficult to obtain, a quick comparison of the ¹H NMR spectra above and below the critical concentration (Fig. 7A) suggests there is substantially more monomer (or other low molecular weight species that can be detected by NMR) than would be expected to exist in a simple micelle model. Instead, the hIAPP oligomers appear to share many properties with mesoscopic clusters, which are large (> 50 nm), dynamic, and metastable aggregates formed by the partial phase separation of long-lived smaller complexes from protein monomers in solution.⁷² Unlike detergent-like micelles, mesoscopic clusters typically contain only a small fraction of the available protein in solution.⁷² It is interesting to note that mesoscopic clusters also show Ostwald ripening,⁷³ a process

in which larger clusters grow at the expense of smaller ones as time progresses by a desorption-condensation process.⁷⁴ Since the stability of amyloid fibers is strongly length dependent,⁷⁵ it is possible that such Ostwald ripening can play a role in the initiation of amyloid assembly if larger clusters favor the creation of longer and therefore more stable nuclei. The disappearance of the smaller oligomers upon the creation of the larger micelle-like oligomers (Figs. 7 and 8) is suggestive, but by no means conclusive, of such a mechanism.

Micelle-like oligomer formation may be a general phenomenon for natively unstructured amyloidogenic proteins

Although all experiments on this study were performed on IAPP, it is likely that other amyloidogenic proteins, particularly those which are natively unfolded in the monomeric state,²⁷ also form protein micelles under specific conditions. Amyloid-beta ($A\beta$) is probably the most intensively studied amyloidogenic protein because of its potential link to Alzheimer's disease. A variety of techniques have shown $A\beta_{1-40}$ has a similar monomer/micelle transition as IAPP. Pyrene and surface tension studies revealed micelle-like oligomers form $A\beta_{1-40}$ at a critical concentration of 17 μM which, if formed, cause a sharp increase in the rate of aggregation.⁴⁰ Similar studies performed under different conditions have shown variable values for the critical concentration of $A\beta_{1-40}$ of 25 μM (0.1 M Tris, pH 7.4 20 °C)⁷⁶ and 8 μM (10 mM phosphate buffer, pH is 7.3, 8 μM),⁷⁷ illustrating the role environmental factors may play. Notably the correlation between amyloidogenicity and critical concentration seems to hold even for the dissimilar $A\beta$ and hIAPP sequences; $A\beta$ has a higher critical concentration and greatly slowed aggregation compared to hIAPP under the same conditions.⁷⁸⁻⁷⁹ Micelles of $A\beta_{1-40}$ have also been directly detected by small angle neutron scattering.³⁹ The SANS experiment show spherocylindrical structures with a radius of 2.4 nm and a length of 11 nm 4 °C and 100 mM DCl (pH 1).³⁹ To the best of our knowledge, a critical temperature has not been detected for $A\beta_{1-40}$,⁸⁰ although the sensitivity of aggregation to environmental conditions does not mean such a critical temperature does not exist, at least under some conditions.

Although the evidence is most clear for $A\beta$ and IAPP, some indirect evidence also exists for micelle formation for other natively unfolded amyloidogenic proteins. Calcitonin, for example, shows the characteristic oligomer peak in its NMR spectra at 1000 μM but not 400 μM at pH 2, indicating a possible micelle-like transition in this range.⁵⁷ Transferred NOEs from the oligomer to monomer allowed a partial reconstruction of the oligomeric structure, which has a turn structure not present in the monomer.⁵⁷ Interestingly, EGCG was shown to completely abolish formation of the calcitonin oligomer.⁵⁷ This observation suggests micelle like oligomers may be targeted by aggregation inhibitors to either shift the critical concentration for oligomer formation or abolish it completely.

Implications of critical concentrations in experimental design

The CMC both hIAPP and $A\beta$ lies in the low micromolar range where many biochemical experiments are performed, which may lead to apparently conflicting interpretations depending on the concentration used. For example, an increase in concentration from 15 to 20 μM leads to a 33% reduction in $t_{1/2}$. By contrast, a much larger increase from 2

to 10 μM results in an essentially negligible change. Because the critical concentration may be influenced by environmental factors, as seen here by changes in pH, changes in environmental conditions may lead to large changes in rate if the critical concentration is crossed. For example, IAPP⁸¹ and other natively unfolded amyloidogenic proteins^{20–21, 56, 82} frequently have a surprisingly large sensitivity to changes in buffer with the rate usually scaling with activity of ions within the Hofmeister series. Buffer sensitivity makes sense in light of the role interfacial tension has in determining the stability of a micelle-like oligomer. Notably, Hofmeister water structure making/breaking effects appear to play a smaller role in IAPP at pH 5.5 where micelle-like oligomers could not be detected in our experiments.⁸¹

Some of the reported variability in the aggregation of these proteins may actually be a result of a switching of the mechanism as a result of crossing the critical points involved in concentration. The mechanism of hIAPP aggregation specifically has been a source of controversy. Real time NMR experiments of hIAPP at pH 6 and 4 °C by Mishra et al have shown the peaks for individual residues do not disappear uniformly as aggregation progresses.⁸³ Instead, the N-terminal cross-peaks disappear before the C-terminal cross-peaks, implying that the formation of large aggregates that are invisible to NMR begins with the formation of N-terminal contacts⁸³, matching well with several other studies showing hIAPP self-association within the N-terminal region.⁸⁴

On the other hand, a parallel 2D-FTIR study at higher temperature and neutral pH suggests that β -sheet formation under these conditions begins in the central region of the peptide, rather than the N-terminus, implying amyloid assembly by IAPP under these conditions is distinctly different than amyloid assembly at low pH and lower temperatures.⁸⁵ The DEST experiment shows these apparent discrepancies may reflect the existence of different oligomers above and below the critical temperature. Below the critical temperature, we see limited association entirely within the N-terminal region, as was observed in Mishra's et al's NMR experiments.⁸³ Above the critical temperature, the DEST interaction profile indicates a much more prominent role for self-association in the central region, in agreement with the 2D-FTIR study. A third mechanism involving initial oligomer formation by the interaction of H18 with the C-terminus has been reported at pH 6 and 25 °C,³⁰ indicating there may be regions in the phase diagram of hIAPP that remain to be explored. Although pyrene fluorescence has potential for screening purposes, there is significant room for improvement in the design of chemical probe for micelle-like and other types of oligomers. In particular, pyrene has very low solubility, which limits many types of binding studies, and the UV detected fluorescence is not easy to adapt to a microplate format. The development of a more soluble fluorophore with excitation in the visible range would allow high throughput screening to map more completely the phase diagram of hIAPP aggregation.

A similar switch in mechanism with concentration has also been observed with $\text{A}\beta_{1-42}$. In a narrow concentration range (20–25 μM) globular $\text{A}\beta_{1-42}$ oligomers formed after that were positive for the oligomer specific A11 antibody and showed a high capacity to disrupt lipid bilayers.⁸⁶ By contrast, at higher concentrations a different type of oligomer was formed that did not react with the A11 antibody that did not disrupt lipid bilayers, despite having a similar size and secondary structure at low concentrations (<20 μM).⁸⁶ Studies such as these show the importance of recognizing the influence of concentration dependent

mechanistic changes and the need for accurate concentration measurements before the start of experiments to minimize batch-to-batch variation and apparent irreproducibility. In this context, it is important to note that some commercial preparations of amyloidogenic peptides made by chemical synthesis contain high levels of salt (in some cases in excess of 50% wt) that can vary substantially from lot to lot.

Although many biochemical experiments are performed in the micromolar range, the physiological concentration of most amyloidogenic proteins is much lower, usually in the pico- to nanomolar range.^{87–88} This concentration range that has been largely unexplored, with the exception of several single-molecule studies^{89–92} and a few other types of studies.²⁵ However, while the circulating concentrations of amyloid peptides is frequently very low, transient concentrations can be quite high in some situations. For example, extracellular A β may be internalized by endocytosis or phagocytosis and trafficked to multivesicular bodies.⁹³ Within these bodies, A β can reach a concentration two orders of magnitude higher than the circulating concentration.⁸⁷

There are several reasons to believe the critical concentration phenomenon may be relevant aggregation for IAPP under physiological conditions. First, the critical concentration for hIAPP (the naturally occurring form) is very low (~2 μ M for the naturally occurring amidated form, Fig. 1). Second, hIAPP is initially stored at millimolar local concentrations in a stable form at low pH⁹⁴ before being diluted to picomolar levels in the blood stream.⁹⁵ This is far in excess of the critical concentration for oligomer formation reported here, and suggests IAPP undergoes at least one passage through the critical concentration before dilution in the bloodstream. Critical concentration phenomena may also be important *in vivo* for other amyloidogenic proteins that occur at high concentrations such as SEVI.⁹⁶

Supplementary Material

Refer to Web version on PubMed Central for supplementary material.

Acknowledgements:

The authors thank Dr. Nicholas Fawzi for assistance with the DEST like experiments.

References

1. Ross CA; Poirier MA, Protein Aggregation and Neurodegenerative Disease. Nat. Med 2004, 10, S10–S17. [PubMed: 15272267]
2. Harrison RS; Sharpe PC; Singh Y; Fairlie DP, Amyloid Peptides and Proteins in Review. Rev. Physiol. Biochem. Pharm 2007, 159, 1–77.
3. Hamley IW, The Amyloid Beta Peptide: A Chemist's Perspective. Role in Alzheimer's and Fibrillization. Chem. Rev 2012, 112, 5147–5192. [PubMed: 22813427]
4. Marchesi VT, Alzheimer's Disease 2012: The Great Amyloid Gamble. Am. J. Pathol 2012, 180, 1762–1767. [PubMed: 22472273]
5. Liu TY; Bitan G, Modulating Self-Assembly of Amyloidogenic Proteins as a Therapeutic Approach for Neurodegenerative Diseases: Strategies and Mechanisms. ChemMedChem 2012, 7, 359–374. [PubMed: 22323134]

6. Hortschansky P; Schroeckh V; Christopeit T; Zandomenighi G; Fandrich M, The Aggregation Kinetics of Alzheimer's Beta-Amyloid Peptide Is Controlled by Stochastic Nucleation. *Protein Sci* 2005, 14, 1753–1759. [PubMed: 15937275]
7. Giehm L; Otzen DE, Strategies to Increase the Reproducibility of Protein Fibrillization in Plate Reader Assays. *Anal. Biochem* 2010, 400, 270–281. [PubMed: 20149780]
8. Teplow DB, On the Subject of Rigor in the Study of Amyloid Beta-Protein Assembly. *Alzheimers Res. Ther* 2013, 5,39. [PubMed: 23981712]
9. Veeraraghavalu K; Zhang C; Miller S; Hefendehl JK; Rajapaksha TW; Ulrich J; Jucker M; Holtzman DM; Tanzi RE; Vassar R, et al. , Comment on “ApoE-Directed Therapeutics Rapidly Clear Beta-Amyloid and Reverse Deficits in AD Mouse Models”. *Science* 2013, 340, 924.
10. Tesseur I; Lo AC; Roberfroid A; Dietvorst S; Van Broeck B; Borgers M; Gijzen H; Moechars D; Mercken M; Kemp J, et al. , Comment on “ApoE-Directed Therapeutics Rapidly Clear Beta-Amyloid and Reverse Deficits in AD Mouse Models”. *Science* 2013, 340, 924.
11. Landreth GE; Cramer PE; Lakner MM; Cirrito JR; Wesson DW; Brunden KR; Wilson DA, Response to Comments on “ApoE-Directed Therapeutics Rapidly Clear Beta-Amyloid and Reverse Deficits in Ad Mouse Models”. *Science* 2013, 340, 924.
12. Price AR; Xu GL; Siemienski ZB; Smithson LA; Borchelt DR; Golde TE; Felsenstein KM, Comment on “ApoE-Directed Therapeutics Rapidly Clear Beta-Amyloid and Reverse Deficits in AD Mouse Models”. *Science* 2013, 340, 924.
13. Fitz NF; Cronican AA; Lefterov I; Koldamova R, Comment on “ApoE-Directed Therapeutics Rapidly Clear Beta-Amyloid and Reverse Deficits in AD Mouse Models”. *Science* 2013, 340, 924.
14. Cramer PE; Cirrito JR; Wesson DW; Lee CYD; Karlo JC; Zinn AE; Casali BT; Restivo JL; Goebel WD; James MJ, et al. , ApoE-Directed Therapeutics Rapidly Clear Beta-Amyloid and Reverse Deficits in AD Mouse Models. *Science* 2012, 335, 1503–1506. [PubMed: 22323736]
15. Pimplikar SW, Reassessing the Amyloid Cascade Hypothesis of Alzheimer's Disease. *Int. J. Biochem. Cell B* 2009, 41, 1261–1268.
16. Benilova I; Karran E; De Strooper B, The Toxic A β Oligomer and Alzheimer's Disease: An Emperor in Need of Clothes. *Nat. Neurosci* 2012, 15, 349–357. [PubMed: 22286176]
17. Haataja L; Gurlo T; Huang CJ; Butler PC, Islet Amyloid in Type 2 Diabetes, and the Toxic Oligomer Hypothesis. *Endocr. Rev* 2008, 29, 303–316. [PubMed: 18314421]
18. Fandrich M, Oligomeric Intermediates in Amyloid Formation: Structure Determination and Mechanisms of Toxicity. *J. Mol. Biol* 2012, 421, 427–440. [PubMed: 22248587]
19. Haass C; Selkoe DJ, Soluble Protein Oligomers in Neurodegeneration: Lessons from the Alzheimer's Amyloid Beta-Peptide. *Nat. Rev. Mol. Cell. Bio* 2007, 8, 101–112. [PubMed: 17245412]
20. Garvey M; Tepper K; Haupt C; Knupfer U; Klement K; Meinhardt J; Horn U; Balbach J; Fandrich M, Phosphate and HEPES Buffers Potently Affect the Fibrillation and Oligomerization Mechanism of Alzheimer's A β Peptide. *Biochem. Biophys. Res. Comm* 2011, 409, 385–388. [PubMed: 21575606]
21. Olsen JS; DiMaio JTM; Doran TM; Brown C; Nilsson BL; Dewhurst S, Seminal Plasma Accelerates Semen-Derived Enhancer of Viral Infection (SEVI) Fibril Formation by the Prostatic Acid Phosphatase (Pap(248–286)) Peptide. *J. Biol. Chem* 2012, 287, 11842–11849. [PubMed: 22354963]
22. Pronchik J; He XL; Giurleo JT; Talaga DS, In Vitro Formation of Amyloid from Alpha-Synuclein Is Dominated by Reactions at Hydrophobic Interfaces. *J. Am. Chem. Soc* 2010, 132, 9797–9803. [PubMed: 20578692]
23. Teplow DB, Preparation of Amyloid Beta-Protein for Structural and Functional Studies. *Meth. Enzymol* 2006, 413, 20–33.
24. Stine WB; Jungbauer L; Yu CJ; Ladu MJ, Preparing Synthetic a Beta in Different Aggregation States. *Meth. Mol. Biol* 2011, 670, 13–32.
25. Hellstrand E; Boland B; Walsh DM; Linse S, Amyloid Beta-Protein Aggregation Produces Highly Reproducible Kinetic Data and Occurs by a Two-Phase Process. *ACS Chem. Neurosci* 2010, 1, 13–18. [PubMed: 22778803]

26. Westermark P; Andersson A; Westermark GT, Islet Amyloid Polypeptide, Islet Amyloid, and Diabetes Mellitus. *Physiol Rev* 2011, 91, 795–826. [PubMed: 21742788]
27. Uversky VN; Fink AL, Conformational Constraints for Amyloid Fibrillation: The Importance of Being Unfolded. *Biochim. Biophys. Acta* 2004, 1698, 131–153. [PubMed: 15134647]
28. Yonemoto IT; Kroon GJ; Dyson HJ; Balch WE; Kelly JW, Amylin Proprotein Processing Generates Progressively More Amyloidogenic Peptides That Initially Sample the Helical State. *Biochemistry* 2008, 47, 9900–9910. [PubMed: 18710262]
29. Tu L-H; Serrano Arnaldo L.; Zanni Martin T.; Raleigh Daniel P., Mutational Analysis of Preamyloid Intermediates: The Role of His-Tyr Interactions in Islet Amyloid Formation. *Biophys. J* 2014, 106, 1520–1527. [PubMed: 24703313]
30. Wei L; Jiang P; Xu WX; Li H; Zhang H; Yan LY; Chan-Park MB; Liu XW; Tang K; Mu YG, et al. , The Molecular Basis of Distinct Aggregation Pathways of Islet Amyloid Polypeptide. *J. Biol. Chem* 2011, 286, 6291–6300. [PubMed: 21148563]
31. Padrick SB; Miranker AD, Islet Amyloid Polypeptide: Identification of Long-Range Contacts and Local Order on the Fibrillogenesis Pathway. *J. Mol. Biol* 2001, 308, 783–794. [PubMed: 11350174]
32. Nanga RPR; Brender JR; Vivekanandan S; Ramamoorthy A, Structure and Membrane Orientation of IAPP in Its Natively Amidated Form at Physiological pH in a Membrane Environment. *Biochim. Biophys. Acta* 2011, 1808, 2337–2342. [PubMed: 21723249]
33. Lomakin A; Chung DS; Benedek GB; Kirschner DA; Teplow DB, On the Nucleation and Growth of Amyloid Beta-Protein Fibrils: Detection of Nuclei and Quantitation of Rate Constants. *Proc. Natl. Acad. Sci. USA* 1996, 93, 1125–1129. [PubMed: 8577726]
34. Lomakin A; Teplow DB; Kirschner DA; Benedek GB, Kinetic Theory of Fibrillogenesis of Amyloid Beta-Protein. *Proc. Natl. Acad. Sci. USA* 1997, 94, 7942–7947. [PubMed: 9223292]
35. Kashchiev D; Cabriolu R; Auer S, Confounding the Paradigm: Peculiarities of Amyloid Fibril Nucleation. *J. Am. Chem. Soc* 2013, 135, 1531–1539. [PubMed: 23305200]
36. Pellarin R; Friedman R; Caflich A, Amyloid Aggregation on Lipid Bilayers and Its Impact on Membrane Permeability. *J Mol Biol* 2009, 387, 407–415. [PubMed: 19133272]
37. Oosawa F; Asakura S, Thermodynamics of the Polymerization of Protein. Academic Press: London; New York, 1975, pg. 204.
38. Hong L; Qi XH; Zhang Y, Dissecting the Kinetic Process of Amyloid Fiber Formation through Asymptotic Analysis. *J. Phys. Chem. B* 2012, 116, 6611–6617. [PubMed: 22126094]
39. Yong W; Lomakin A; Kirkitadze MD; Teplow DB; Chen SH; Benedek GB, Structure Determination of Micelle-Like Intermediates in Amyloid Beta-Protein Fibril Assembly by Using Small Angle Neutron Scattering. *Proc. Natl. Acad. Sci. USA* 2002, 99, 150–154. [PubMed: 11756677]
40. Sabate R; Estelrich J, Evidence of the Existence of Micelles in the Fibrillogenesis of Beta-Amyloid Peptide. *J. Phys. Chem. B* 2005, 109, 11027–11032. [PubMed: 16852343]
41. Rhoades E; Gafni A, Micelle Formation by a Fragment of Human Islet Amyloid Polypeptide. *Biophys. J* 2003, 84, 3480–3487. [PubMed: 12719273]
42. Jean L; Lee CF; Lee C; Shaw M; Vaux DJ, Competing Discrete Interfacial Effects Are Critical for Amyloidogenesis. *FASEB J.* 2010, 24, 309–317. [PubMed: 19741169]
43. Padrick SB; Miranker AD, Islet Amyloid: Phase Partitioning and Secondary Nucleation Are Central to the Mechanism of Fibrillogenesis. *Biochemistry* 2002, 41, 4694–4703. [PubMed: 11926832]
44. Rhoades E; Agarwal J; Gafni A, Aggregation of an Amyloidogenic Fragment of Human Islet Amyloid Polypeptide. *Biochim. Biophys. Acta* 2000, 1476, 230–238. [PubMed: 10669788]
45. Kalyanasundaram K; Thomas JK, Environmental Effects on Vibronic Band Intensities in Pyrene Monomer Fluorescence and Their Application in Studies of Micellar Systems. *J. Am. Chem. Soc* 1977, 99, 2039–2044.
46. Ruiz CC; Aguiar J; Carpena P; Molina-Bolivar JA, On the Determination of the Critical Micelle Concentration by the Pyrene 1 : 3 Ratio Method. *J. Colloid Interface Sci* 2003, 258, 116–122.

47. Reinke AA; Ung PMU; Quintero JJ; Carlson HA; Gestwicki JE, Chemical Probes That Selectively Recognize the Earliest A β Oligomers in Complex Mixtures. *J. Am. Chem. Soc* 2010, 132, 17655–17657. [PubMed: 21105683]
48. Israelachvili JN, *Intermolecular and Surface Forces*. 3rd ed.; Academic Press: Burlington, MA, 2011, pg. 674
49. Jan A; Hartley DM; Lashuel HA, Preparation and Characterization of Toxic A β Aggregates for Structural and Functional Studies in Alzheimer's Disease Research. *Nat. Protoc* 2010, 5, 1186–1209. [PubMed: 20539293]
50. Pan J; Han J; Borchers CH; Konermann L, Structure and Dynamics of Small Soluble A β (1–40) Oligomers Studied by Top-Down Hydrogen Exchange Mass Spectrometry. *Biochemistry* 2012, 51, 3694–3703. [PubMed: 22486153]
51. Woodbury RL; Hardy SJ; Randall LL, Complex Behavior in Solution of Homodimeric Seca. *Protein Sci* 2002, 11, 875–882. [PubMed: 11910030]
52. Barbar E, NMR Characterization of Partially Folded and Unfolded Conformational Ensembles of Proteins. *Biopolymers* 1999, 51, 191–207. [PubMed: 10516571]
53. Brender JR; Hartman K; Reid KR; Kennedy RT; Ramamoorthy A, A Single Mutation in the Nonamyloidogenic Region of Islet Amyloid Polypeptide Greatly Reduces Toxicity. *Biochemistry* 2008, 47, 12680–12688. [PubMed: 18989933]
54. Cao P; Abedini A; Wang H; Tu LH; Zhang X; Schmidt AM; Raleigh DP, Islet Amyloid Polypeptide Toxicity and Membrane Interactions. *Proc. Natl. Acad. Sci. USA* 2013, 110, 19279–19284. [PubMed: 24218607]
55. Radovan D; Smirnovas V; Winter R, Effect of Pressure on Islet Amyloid Polypeptide Aggregation: Revealing the Polymorphic Nature of the Fibrillation Process. *Biochemistry* 2008, 47, 6352–6360. [PubMed: 18498175]
56. Narayanan S; Reif B, Characterization of Chemical Exchange between Soluble and Aggregated States of Beta-Amyloid by Solution-State NMR Upon Variation of Salt Conditions. *Biochemistry* 2005, 44, 1444–1452. [PubMed: 15683229]
57. Huang R; Vivekanandan S; Brender JR; Abe Y; Naito A; Ramamoorthy A, NMR Characterization of Monomeric and Oligomeric Conformations of Human Calcitonin and Its Interaction with EGCG. *J. Mol. Biol* 2012, 416, 108–120. [PubMed: 22200484]
58. Krishnamoorthy J; Brender JR; Vivekanandan S; Jahr N; Ramamoorthy A, Side-Chain Dynamics Reveals Transient Association of A β (1–40) Monomers with Amyloid Fibers. *J. Phys. Chem. B* 2012, 116, 13618–13623. [PubMed: 23116141]
59. Dorgere B; Khemtemourian L; Correia I; Soulier JL; Lequin O; Ongeri S, Sugar-Based Peptidomimetics Inhibit Amyloid Beta-Peptide Aggregation. *European Journal of Medicinal Chemistry* 2011, 46, 5959–5969. [PubMed: 22027101]
60. Soong R; Brender JR; Macdonald PM; Ramamoorthy A, Association of Highly Compact Type II Diabetes Related Islet Amyloid Polypeptide Intermediate Species at Physiological Temperature Revealed by Diffusion NMR Spectroscopy. *J. Am. Chem. Soc* 2009, 131, 7079–7085. [PubMed: 19405534]
61. Fawzi NL; Ying J; Torchia DA; Clore GM, Kinetics of Amyloid Beta Monomer-to-Oligomer Exchange by Nmr Relaxation. *J. Am. Chem. Soc* 2010, 132, 9948–9951. [PubMed: 20604554]
62. Fawzi NL; Ying JF; Ghirlando R; Torchia DA; Clore GM, Atomic-Resolution Dynamics on the Surface of Amyloid-Beta Protofibrils Probed by Solution NMR. *Nature* 2011, 480, 268–272. [PubMed: 22037310]
63. Fawzi NL; Ying JF; Torchia DA; Clore GM, Probing Exchange Kinetics and Atomic Resolution Dynamics in High-Molecular-Weight Complexes Using Dark-State Exchange Saturation Transfer Nmr Spectroscopy. *Nat. Protoc* 2012, 7, 1523–1533. [PubMed: 22814391]
64. Esposito V; Das R; Melacini G, Mapping Polypeptide Self-Recognition through H-1 Off-Resonance Relaxation. *J. Am. Chem. Soc* 2005, 127, 9358–9359. [PubMed: 15984849]
65. Algamil M; Milojevic J; Jafari N; Zhang W; Melacini G, Mapping the Interactions between the Alzheimer's A β -Peptide and Human Serum Albumin Beyond Domain Resolution. *Biophys. J* 2013, 105, 1700–1709. [PubMed: 24094411]

66. Milojevic J; Costa M; Ortiz AM; Jorquera JI; Melacini G, In Vitro Amyloid-Beta Binding and Inhibition of Amyloid-Beta Self-Association by Therapeutic Albumin. *J. Alzheimer's Dis* 2014, 38, 753–765. [PubMed: 24072068]
67. Milojevic J; Melacini G, Stoichiometry and Affinity of the Human Serum Albumin-Alzheimer's Abeta Peptide Interactions. *Biophys. J* 2011, 100, 183–92. [PubMed: 21190670]
68. Milojevic J; Raditsis A; Melacini G, Human Serum Albumin Inhibits Abeta Fibrillization through a “Monomer-Competitor” Mechanism. *Biophys. J* 2009, 97, 2585–2594. [PubMed: 19883602]
69. Raditsis AV; Milojevic J; Melacini G, A β Association Inhibition by Transferrin. *Biophys. J* 2013, 105, 473–480. [PubMed: 23870268]
70. Abedini A; Meng FL; Raleigh DP, A Single-Point Mutation Converts the Highly Amyloidogenic Human Islet Amyloid Polypeptide into a Potent Fibrillization Inhibitor. *J. Am. Chem. Soc* 2007, 129, 11300–11301. [PubMed: 17722920]
71. Buchanan LE; Dunkelberger EB; Tran HQ; Cheng PN; Chiu CC; Cao P; Raleigh DP; de Pablo JJ; Nowick JS; Zanni MT, Mechanism of IAPP Amyloid Fibril Formation Involves an Intermediate with a Transient Beta-Sheet. *Proc. Natl. Acad. Sci. USA* 2013, 110, 19285–19290. [PubMed: 24218609]
72. Pan W; Vekilov PG; Lubchenko V, Origin of Anomalous Mesoscopic Phases in Protein Solutions. *J. Phys. Chem. B* 2010, 114, 7620–7630. [PubMed: 20423058]
73. Li Y; Lubchenko V; Vorontsova MA; Filobelo L; Vekilov PG, Ostwald-Like Ripening of the Anomalous Mesoscopic Clusters in Protein Solutions. *J. Phys. Chem. B* 2012, 116, 10657–10664. [PubMed: 22889282]
74. Lifshitz IM; Slyozov VV, The Kinetics of Precipitation from Supersaturated Solid Solutions. *J. Phys. Chem. Solids* 1961, 19, 35–50.
75. Linse B; Linse S, Monte Carlo Simulations of Protein Amyloid Formation Reveal Origin of Sigmoidal Aggregation Kinetics. *Mol. Biosys* 2011, 7, 2296–2303.
76. Soreghan B; Kosmoski J; Glabe C, Surfactant Properties of Alzheimer's a Beta Peptides and the Mechanism of Amyloid Aggregation. *J. Biol. Chem* 1994, 269, 28551–28554. [PubMed: 7961799]
77. Lei LZ, PhD Thesis. Mechanism of Early Stage Abeta Amyloid Formation. Case Western Reserve University, 2008.
78. Suzuki Y; Brender JR; Hartman K; Ramamoorthy A; Marsh ENG, Alternative Pathways of Human Islet Amyloid Polypeptide Aggregation Distinguished by F-19 Nuclear Magnetic Resonance-Detected Kinetics of Monomer Consumption. *Biochemistry* 2012, 51, 8154–8162. [PubMed: 22998665]
79. Suzuki Y; Brender JR; Soper MT; Krishnamoorthy J; Zhou YL; Ruotolo BT; Kotov NA; Ramamoorthy A; Marsh ENG, Resolution of Oligomeric Species During the Aggregation of A β (1–40) Using F-19 Nmr. *Biochemistry* 2013, 52, 1903–1912. [PubMed: 23445400]
80. Kusumoto Y; Lomakin A; Teplov DB; Benedek GB, Temperature Dependence of Amyloid Beta-Protein Fibrillization. *Proc. Natl. Acad. Sci. USA* 1998, 95, 12277–12282. [PubMed: 9770477]
81. Marek PJ; Patsalo V; Green DF; Raleigh DP, Ionic Strength Effects on Amyloid Formation by Amylin Are a Complicated Interplay among Debye Screening, Ion Selectivity, and Hofmeister Effects. *Biochemistry* 2012, 51, 8478–8490. [PubMed: 23016872]
82. Yeh V; Broering JM; Romanyuk A; Chen B; Chernoff YO; Bommarius AS, The Hofmeister Effect on Amyloid Formation Using Yeast Prion Protein. *Protein Sci* 2010, 19, 47–56. [PubMed: 19890987]
83. Mishra R; Geyer M; Winter R, Nmr Spectroscopic Investigation of Early Events in IAPP Amyloid Fibril Formation. *Chembiochem* 2009, 10, 1769–72. [PubMed: 19575373]
84. Mazor Y; Gilead S; Benhar I; Gazit E, Identification and Characterization of a Novel Molecular-Recognition and Self-Assembly Domain within the Islet Amyloid Polypeptide. *J. Mol. Biol* 2002, 322, 1013–1024. [PubMed: 12367525]
85. Shim SH; Gupta R; Ling YL; Strasfeld DB; Raleigh DP; Zanni MT, Two-Dimensional IR Spectroscopy and Isotope Labeling Defines the Pathway of Amyloid Formation with Residue-Specific Resolution. *Proc. Natl. Acad. Sci. USA* 2009, 106, 6614–6619. [PubMed: 19346479]

86. Ladiwala ARA; Litt J; Kane RS; Aucoin DS; Smith SO; Ranjan S; Davis J; Van Nostrand WE; Tessier PM, Conformational Differences between Two Amyloid Beta Oligomers of Similar Size and Dissimilar Toxicity. *J. Biol. Chem* 2012, 287, 24765–24773. [PubMed: 22547072]
87. Hu XY; Crick SL; Bu GJ; Frieden C; Pappu RV; Lee JM, Amyloid Seeds Formed by Cellular Uptake, Concentration, and Aggregation of the Amyloid-Beta Peptide. *Proc. Natl. Acad. Sci. USA* 2009, 106, 20324–20329. [PubMed: 19910533]
88. Kuo YM; Emmerling MR; Lampert HC; Hempelman SR; Kokjohn TA; Woods AS; Cotter RJ; Roher AE, High Levels of Circulating Abeta42 Are Sequestered by Plasma Proteins in Alzheimer's Disease. *Biochem. Biophys. Res. Comm* 1999, 257, 787–791. [PubMed: 10208861]
89. Ding H; Wong PT; Lee EL; Gafni A; Steel DG, Determination of the Oligomer Size of Amyloidogenic Protein Beta-Amyloid(1–40) by Single-Molecule Spectroscopy. *Biophys. J* 2009, 97, 912–921. [PubMed: 19651050]
90. Johnson RD; Schauerte JA; Wissner KC; Gafni A; Steel DG, Direct Observation of Single Amyloid-Beta(1–40) Oligomers on Live Cells: Binding and Growth at Physiological Concentrations. *Plos One* 2011, 6, e23970. [PubMed: 21901146]
91. Sengupta P; Garai K; Sahoo B; Shi Y; Callaway DJE; Maiti S, The Amyloid Beta Peptide (a Beta(1–40)) Is Thermodynamically Soluble at Physiological Concentrations. *Biochemistry* 2003, 42, 10506–10513. [PubMed: 12950178]
92. Nag S; Sarkar B; Bandyopadhyay A; Sahoo B; Sreenivasan VK; Kombrabail M; Muralidharan C; Maiti S, Nature of the Amyloid-Beta Monomer and the Monomer-Oligomer Equilibrium. *J. Biol. Chem* 2011, 286, 13827–33. [PubMed: 21349839]
93. Friedrich RP; Tepper K; Roznicke R; Soom M; Westermann M; Reymann K; Kaether C; Fandrich M, Mechanism of Amyloid Plaque Formation Suggests an Intracellular Basis of A β Pathogenicity. *Proc. Natl. Acad. Sci. USA* 2010, 107, 1942–1947. [PubMed: 20133839]
94. Knight JD; Williamson JA; Miranker AD, Interaction of Membrane-Bound Islet Amyloid Polypeptide with Soluble and Crystalline Insulin. *Protein Sci* 2008, 17, 1850–1856. [PubMed: 18765820]
95. Butler PC; Chou J; Carter WB; Wang YN; Bu BH; Chang D; Chang JK; Rizza RA, Effects of Meal Ingestion on Plasma Amylin Concentration in Niddm and Nondiabetic Humans. *Diabetes* 1990, 39, 752–756. [PubMed: 2189768]
96. Munch J; Rucker E; Standker L; Adermann K; Goffinet C; Schindler M; Wildum S; Chinnadurai R; Rajan D; Specht A, et al. , Semen-Derived Amyloid Fibrils Drastically Enhance HIV Infection. *Cell* 2007, 131, 1059–1071. [PubMed: 18083097]

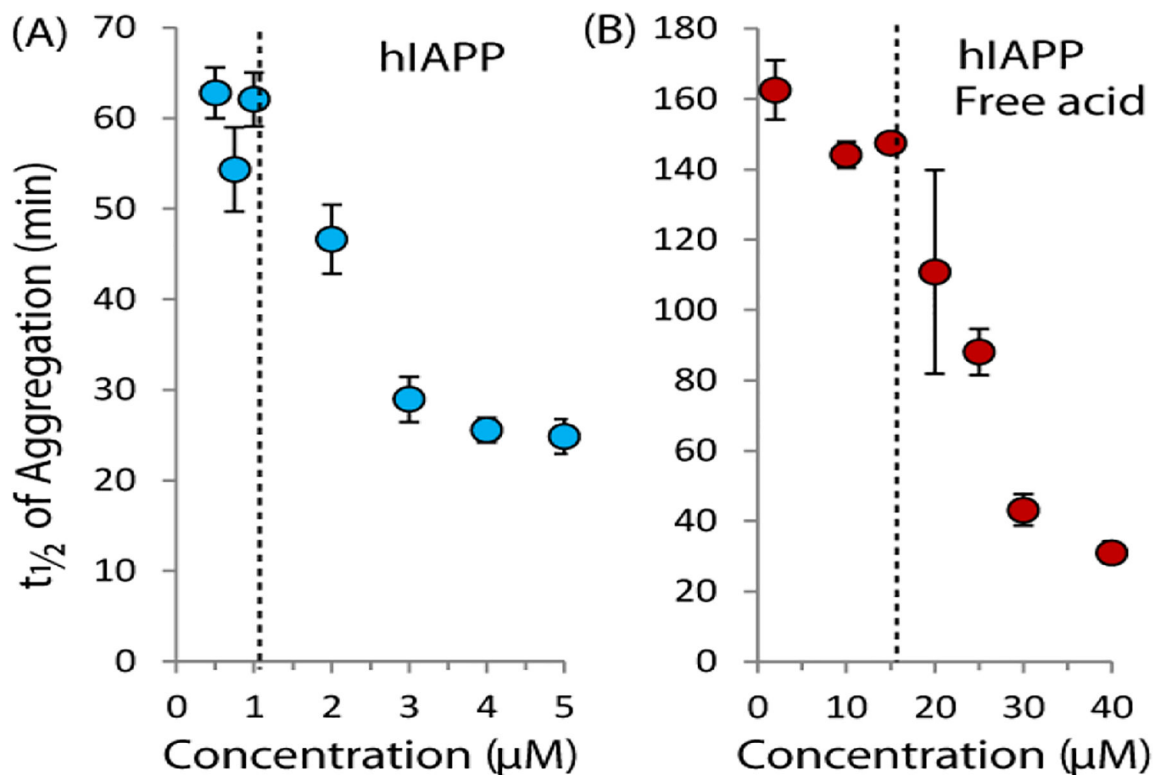


Figure 1. The rate of amyloid formation of hIAPP increases sharply near a threshold concentration.

Time to one half completion of amyloid formation as a function of hIAPP concentration for the native amidated hIAPP sequence (left) and the free acid version (right) as measured by the amyloid specific dye ThT at 25°C with orbital shaking (pH 7.3 10 mM sodium phosphate buffer, 100 mM NaCl). The dashed lines indicate the approximate threshold concentrations from the aggregation experiment. Error bars represent S.E.M. for six (hIAPP) or three (hIAPP free acid) experiments.

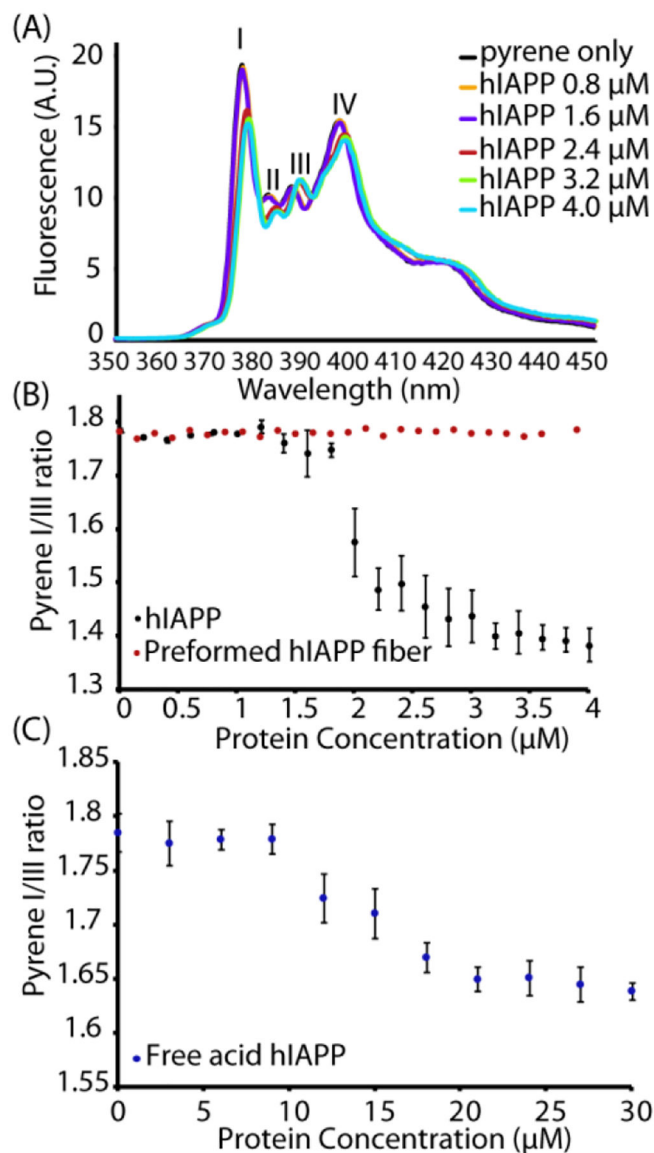


Figure 2. Pyrene specifically detects concentration dependent oligomer formation over amyloid fibers.

(A) Fluorescence emission spectra of 1 μM pyrene with the indicated concentrations of hIAPP upon excitation at 334 nm. (B) Plots of the pyrene I_I/I_{III} ratio measured during a titration with freshly dissolved hIAPP at pH 7.3 (black circles) or preformed fibers of hIAPP (allowed to aggregate beforehand for 24 hours at 37 °C with shaking, red circles). (C) Corresponding plots of the pyrene I_I/I_{III} ratio measured with hIAPP free acid. Note the difference in the x-axis scale from (B). All measurements were performed in phosphate buffer 20 mM, 50 mM NaCl, 1 μM pyrene at 25 °C. Errors bars indicate S.E.M. (measurement preformed in triplicate).

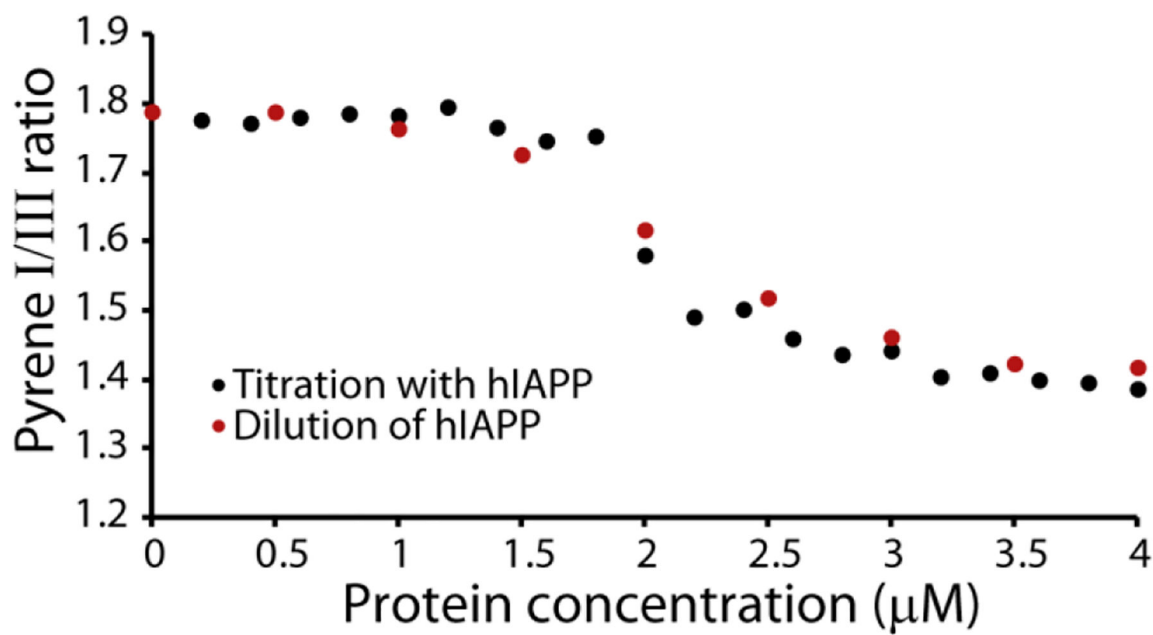


Figure 3. Concentration dependent oligomer formation of hIAPP is reversible.

Plots of the pyrene I_I/I_{III} ratio measured either by titration with freshly dissolved hIAPP at pH 7.3 (black circles) or by dilution from 4 μM hIAPP (red circles). All measures were performed in 20 mM phosphate buffer, 50 mM NaCl, 25 °C. The pyrene concentration is kept constant at 1 μM for all experiments.

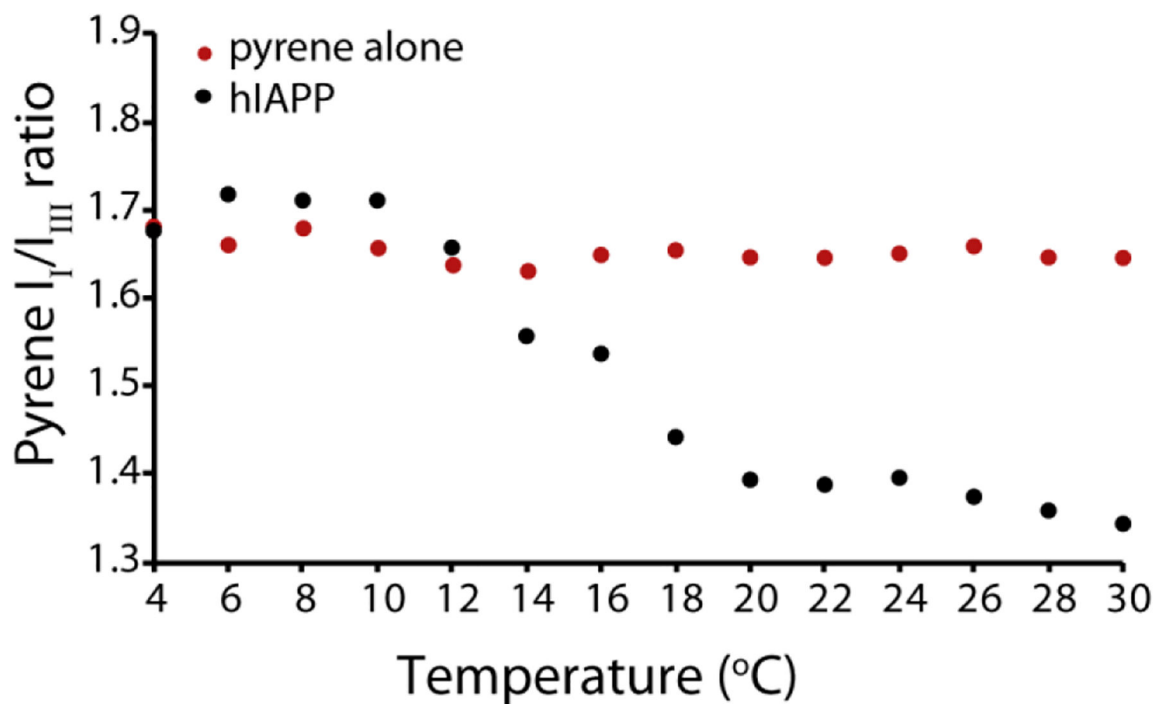


Figure 4. Oligomer formation of hIAPP only occurs above an apparent critical solution temperature.

Plot of the pyrene I_I/I_{III} ratio in the presence of 4 μM hIAPP at pH 7.3 at increasing temperature values (black circles). As control the pyrene I_I/I_{III} ratio in absence of hIAPP was collected (red circles). All measures were performed at pH 7.3 in 20 mM phosphate buffer, 50 mM NaCl, 1 μM pyrene.

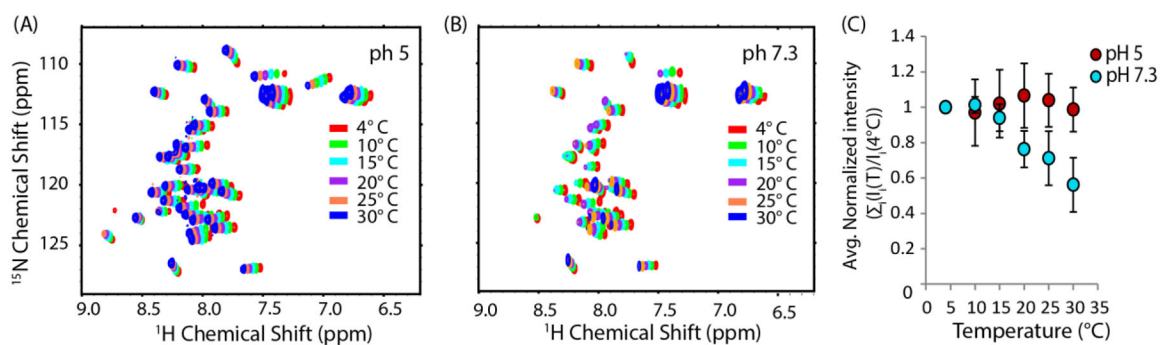


Figure 5. Peak intensity in the NMR spectra of hIAPP free acid sharply decreases at a critical temperature at pH 7.3 but not pH 5.

Temperature dependence of the ^{15}N HSQC spectra of 78 μM hIAPP free acid in 20 mM sodium phosphate buffer, 50 mM NaCl at pH 5 (A) and pH 7.3 (B). (C) Average of the peak intensity relative to the value at 4 $^\circ\text{C}$ as a function of temperature. Error bars represent the S.E.M. considering N to be the number of residues.

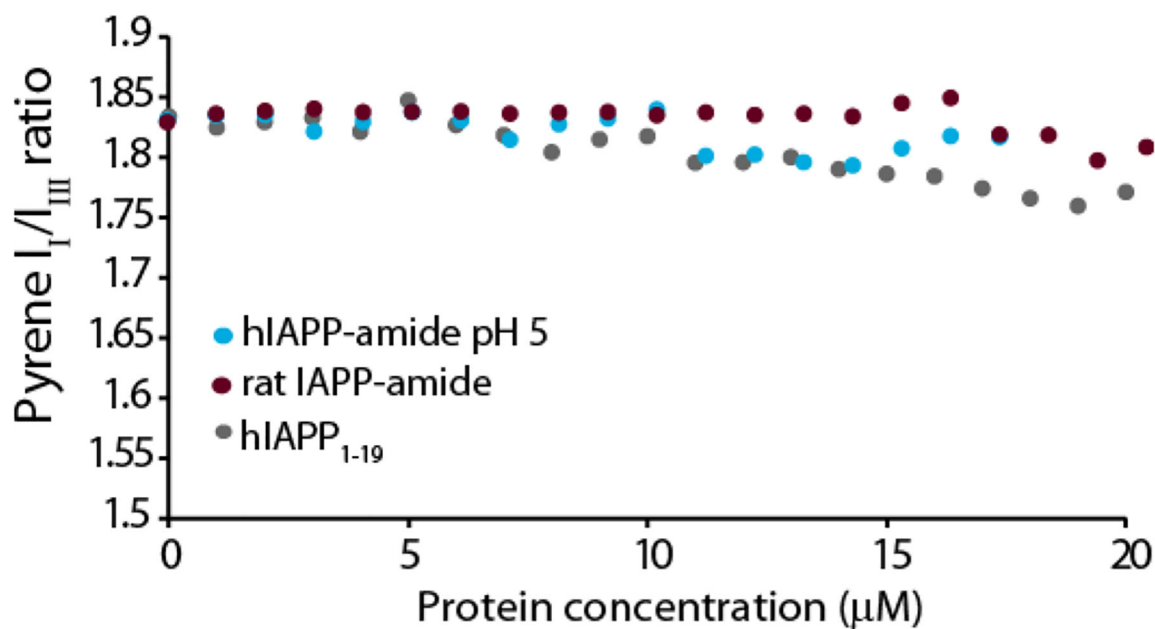


Figure 6. Non- or weakly amyloidogenic IAPP variants do not form pyrene detectable oligomers. Plots of the pyrene II/III ratio measured during a titration with freshly dissolved hIAPP at pH 5 (cyan circles), non-amyloidogenic amidated rat IAPP (maroon circles), or weakly amyloidogenic hIAPP₁₋₁₉ (grey circles). All measures were performed in 20 mM phosphate buffer, 50 mM NaCl, 1 μM pyrene at 25 °C.

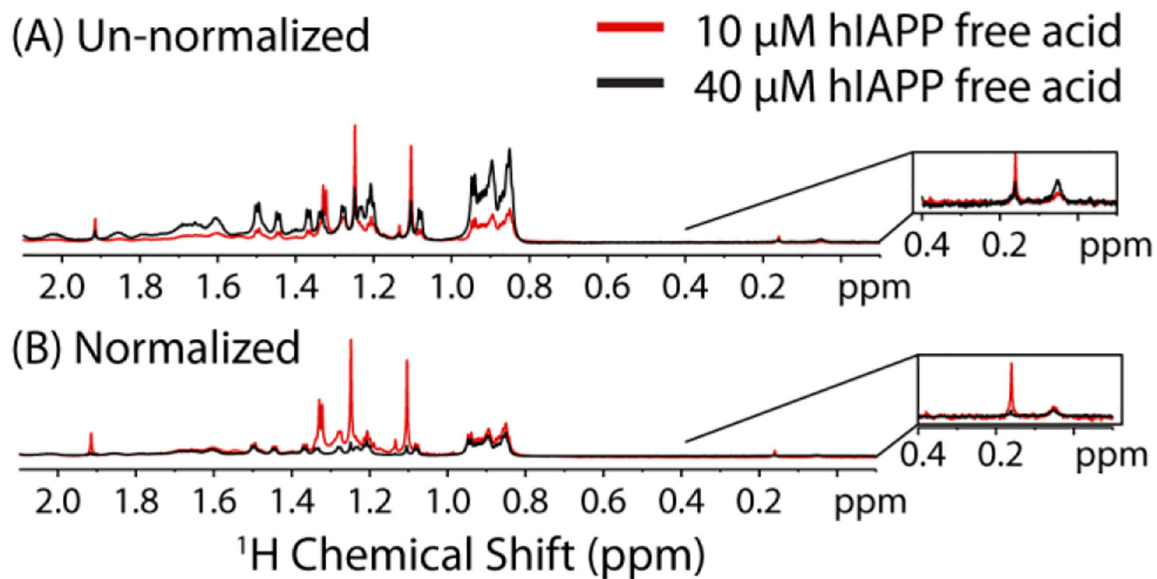


Figure 7. Dilution changes the ^1H NMR spectra of hIAPP free acid.

^1H NMR spectra of 10 and 40 μM hIAPP free acid at 37 $^\circ\text{C}$ in 20 mM sodium phosphate buffer, 50 mM NaCl at pH 7.3 normalized to the number of scans only (A) and normalized to both the concentration and number of scans (B). **Inset** Strongly shielded peaks previously correlated with oligomer formation.

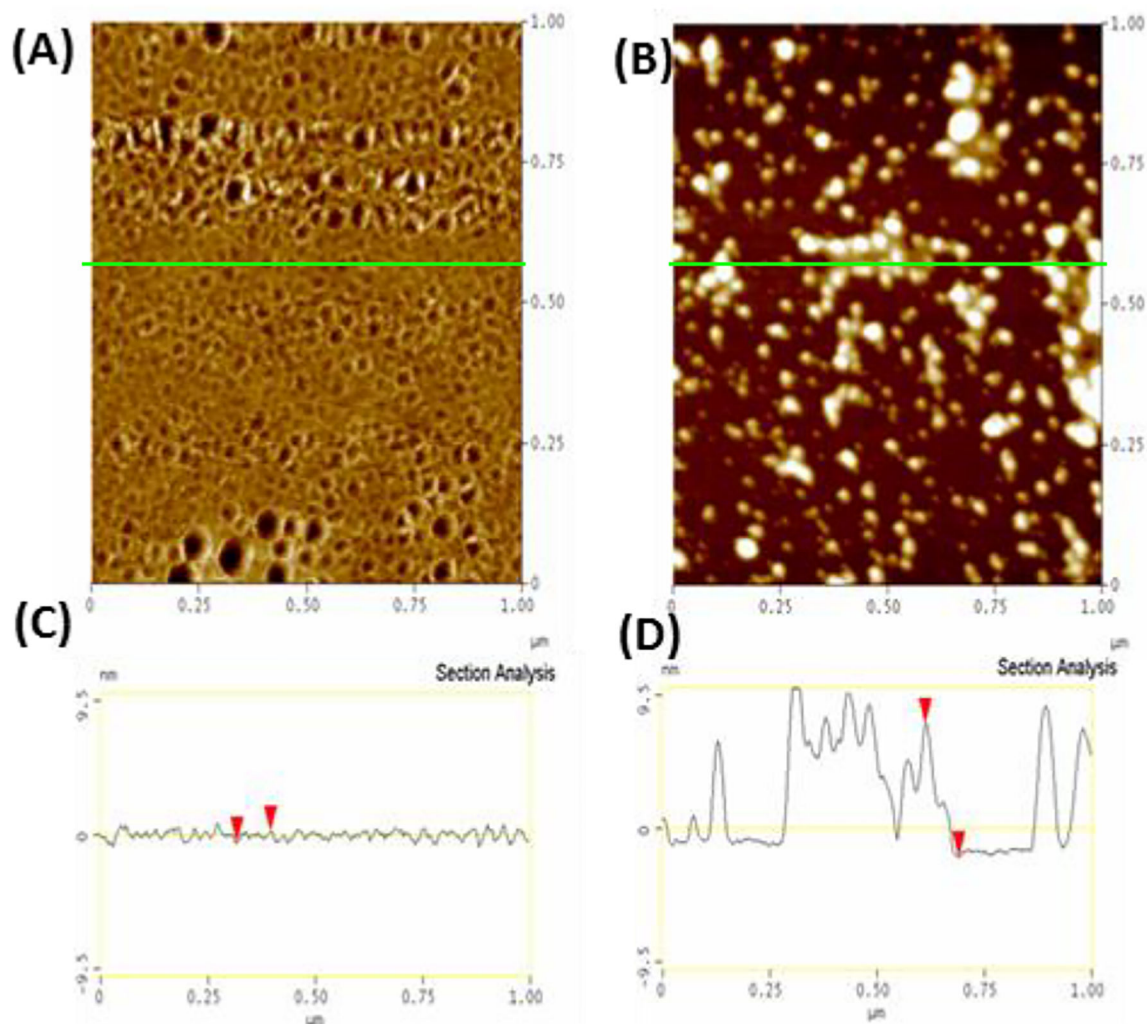


Figure 8. hIAPP forms a different type of oligomer following brief incubation at 4°C or 25°C. **Top** Different aliquots of the same solution of 10 μM hIAPP (initially at 4°C, 10 mM phosphate buffer, 100 mM NaCl, pH 7.4) were either left at 4°C (A) or heated to 25°C (B) and then quickly deposited on SiO₂, frozen with liquid N₂, and then lyophilized to preserve the morphology of the original aggregates and the by tapping mode AFM in air (40% humidity). **Bottom:** Section analysis of samples initially prepared at 4°C (C) and 25°C (D) showing the height distribution along the green line in (A) and (B).

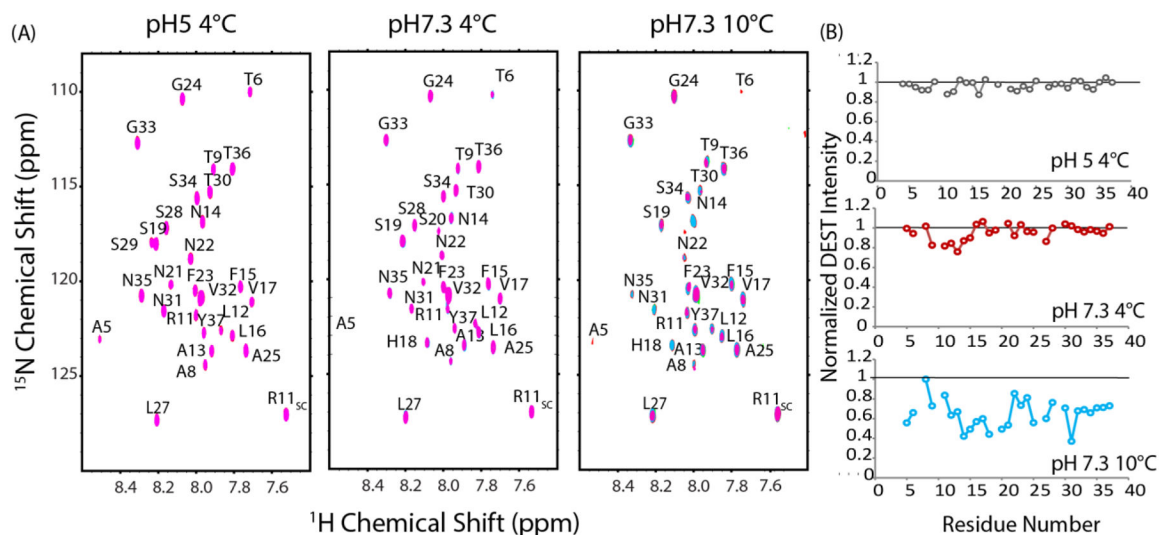


Figure 9. Changes in self-interaction profile with pH and temperature through DEST NMR experiments.

(A) DEST NMR spectra of 78 μM hIAPP free acid at pH 5 and 4°C, pH 7.3 and 4°C (C) pH 7.3 and 10°C in 20 mM phosphate buffer, 50 mM NaCl. Pink contours represent saturation at 30 kHz off-resonance, blue contours from 5 kHz off-resonance saturation. **Right:** Changes in relative intensity upon saturation expressed as the ratio between the intensity at 5 kHz and 30 kHz off-resonance saturation.